



Orbital forcing of dust supply to the North Canary Basin over the last 250 kyr

Ana Moreno^a, Jordi Targarona^a, Jorijntje Henderiks^b, Miquel Canals^{a,*},
Tim Freudenthal^c, Helge Meggers^c

^aGrup de Recerca Consolidat en Geociències Marines, Departament d'Estratigrafia i Paleontologia, Universitat de Barcelona, Campus de Pedralbes, E-08071 Barcelona, Spain

^bSwiss Federal Institute of Technology, Geological Institute, CH-8092 Zürich, Switzerland

^cUniversität Bremen, FB Geowissenschaften, Postfach 33 04 40, D-28359 Bremen, Germany

Abstract

The Canary Basin lies in a region of strong interaction between the atmospheric and ocean circulation systems: Trade winds drive seasonal coastal upwelling and dust storm outbreaks from the neighbouring Sahara desert are the major source of terrigenous sediment. To investigate the forcing mechanisms for dust input and wind strength in the North Canary Basin, the temporal pattern of variability of sedimentological and geochemical proxy records has been analysed in two sediment cores between latitudes 30°30'N and 31°40'N. Spectral analysis of the dust proxy records indicates that insolation changes related to eccentricity and precession are the main periods of temporal variation in the record. Si/Al and grain-size of the terrigenous fraction show an increase in glacial–interglacial transitions while Al concentration and Fe/Al ratio are both in phase with minima in the precessional index. Hence, the results obtained show that the wind strength was intensified at Terminations. At times of maxima of Northern Hemisphere seasonal insolation, when the African monsoon was enhanced, the North Canary Basin also received higher dust input. This result suggests that the moisture brought by the monsoon may have increased the availability of dust in the source region. © 2001 Elsevier Science Ltd. All rights reserved.

1. Introduction

Eolian sediment generated in the world's arid and semiarid regions with persistent dry winds is transported over large distances and contributes to sediment in the ocean basins (Prospero, 1996). Indeed, the Saharan region has been revealed as the major source of dust particles to the deep-sea sediments of the North Atlantic Ocean (Schütz et al., 1981). Sedimentological and geochemical analyses of sediments from deep-sea cores may help to identify variations in continental aridity and wind strength, thus helping to understand mechanisms involved in climate change (see for example Sarnthein et al., 1982; Stein, 1985). Changes in eolian grain size have been used to investigate paleowind pathways off Northwest Africa (Parkin and Shackleton, 1973). Pollen assemblages (Hooghiemstra et al., 1992; Marret and Turon,

1994) and freshwater diatoms (Pokras and Mix, 1985, 1987) in marine cores have also been used as proxies for wind strength. Mass accumulation rates (MAR) of marine sediments free from biogenic and authigenic components, can be used to study eolian sedimentation (Clemens and Prell, 1990). In addition, mineral and geochemical compositions, such as aluminium concentration (Matthewson et al., 1995) or Fe/Al ratio (Bergametti et al., 1989), are useful proxies to monitor changes in aridity of the source areas. Therefore, sedimentological and geochemical studies of deep-sea sediments may provide useful information about paleowind directions and strength and continental climate.

In the study of marine sediments, Kolla et al. (1979) pioneered the use of quartz as an indicator of eolian transport to the Atlantic Ocean. They concluded that the increase of wind strength and aridity were both higher during the Last Glacial Maximum (LGM). Sarnthein et al. (1981) and Hooghiemstra (1989) interpreted that wind strength was enhanced during eccentricity-controlled glacial periods on the basis of grain size and palynological studies. In addition, Ruddiman (1997) proposed that

* Corresponding author. Tel.: + 34-93-402-1360; fax: + 34-93-402-1340.

E-mail address: miquel@natura.geo.ub.es (M. Canals).

the high glacial influx of dust to the tropical Atlantic are mainly due to changes in transport by winter winds, rather than to glacial hyper-aridity. Recently, several authors have highlighted the importance of the local oceanographical conditions in the sedimentological record (Bertrand et al., 1996). In some Northwest African records the higher dust input has been recognised at the Oxygen Isotope Stage (OIS) 2–1 transition (Lézine and Denèfle, 1997; Martinez et al., 1999) thus questioning the assumption that glacial stages were characterised by stronger winds.

Several studies have linked dust input to climate variation in the source areas, thus providing a low-latitude climate response to solar radiation. Matthewson et al. (1995) and Tiedemann et al. (1989) interpret increments in dust supply to an increase in aridity at the source. This hypothesis is based on the relation between the humidity/aridity cycles and the low-latitude insolation forcing of the African monsoon. Therefore, in times of minima in the precessional index, a higher seasonality leads to more intense monsoons (McIntyre et al., 1989). Wet intervals in Northwestern Africa are recorded in lakes concomitantly with intensifications in the monsoonal regime (Kutzbach and Street-Perrott, 1985; Gasse et al., 1989; Lamb et al., 1995). However, after mapping sand-dune extent on North Africa, aridity has been related with Northern Hemisphere glaciations instead of the precessional insolation timing (Sarnthein, 1978). In addition, results from general circulation models (GCM) suggest that ice sheets can affect African climate via changes in sea surface temperatures over the North Atlantic Ocean (deMenocal and Rind, 1993a, b). In conclusion, the tempo of aridity in Northwestern Africa during the Late Pleistocene is still a matter of debate (Ruddiman, 1997).

In summary, the deep-sea sediment recorded under the influence of Saharan dust plumes can provide the key to test the previous hypotheses. The aim of this study is to evaluate to which extent orbital forcing plays a key role driving changes in dust input to the North Canary Basin (NCB). Our wind strength proxies show a variation mainly controlled by the 100-kyr cycle while the dust-input record is modified by the seasonality implied by the precessional insolation timing. Finally, the interpretation of these results leads us to propose a conceptual model to explain the variation of dust supply to the NCB over the last 250 kyr.

2. Oceanographic and climatic setting

The Canary Basin lies in the recirculation regime linking the Gulf Stream with the North Equatorial Current via the Azores and Canary Currents (Klein and Siedler, 1989). At this latitude coastal upwelling is driven by the interaction between the trade winds and the Canary Current. Along the Northwestern African margin, the

trade winds show a pattern of seasonal variations. Thus, dividing the Northwestern African margin into regions of permanent and seasonal upwelling (Wooster et al., 1976; Fütterer, 1983). North of latitude 25°N, the upwelling has a seasonal character, being more active in spring and summer, because of the seasonal shift in the location of the subtropical high-pressure cell, which drives the trades (Mittelstaedt, 1983). Although the upwelling zone is restricted to the coast, satellite image has shown that large upwelling filaments develop at specific coastal positions such as Cape Ghir, Cape Blanc or Cape Yubi (Van Camp et al., 1991; Gabric et al., 1993; Davenport et al., 1999). As a result, the upwelling signal can be transported far offshore.

The NCB is located in the path of long-range atmospheric dust transport offshore the Northwestern Africa (Prospero, 1996). Dust input into this area is controlled by the Northeast Trade winds and the Saharan Air Layer (SAL) wind systems (Sarnthein and Koopmann, 1980). At present, major dust outbreaks that carry dust to the NCB are linked with the northern branch of the SAL wind system (Gelado-Caballero et al., 2000). These observations were also confirmed from modelling results (Tetzlaff and Wolter, 1980) and by the calculations of isentropic back-trajectories after satellite data (Bustos et al., 1998). These Saharan winds transport particles from the rim of the South Sahara and Sahel regions. There the widespread lateritic soils and ferruginous crusts give characteristic high Fe content to the dust (Sarnthein et al., 1981).

The current dust input to the NCB was studied by Gelado-Caballero et al. (2001). These authors have found that the highest occurrence of dust outbreaks take place in winter and summer related to two dominant meteorological scenarios. In winter, dust events occur favoured by the weakening of the Azores High and the Intertropical Convergence Zone (ITCZ) is located southwards. Bergametti et al. (1989) observed dust transport from the Sahelian regions when the incursion of a polar depression cuts the Azores High into two anticyclonic cells, an oceanic and a continental one. In contrast, dust outbreaks appear in summer when the high pressure is centred around the Azores combined with a low-pressure cell over Northern Africa, which favours dust transport from a northern source (Gelado-Caballero et al., 2001).

Up to now, the Sahelian origin of the dust was the most accepted in the literature. However, Chiapello et al. (1997) showed that the low-level summer trade winds transport mineral aerosol from northeastern Morocco to the Canary region. This conclusion opens the possibility that indeed the sediment composition of the North Canary Basin may represent two different sources. The predominance of one source over the other may be related to the prevailing meteorological scenario.

3. Material and methods

The two cores studied, GeoB 4216-1 and GeoB 5559-2, were retrieved during R/V METEOR cruises M37/1 and M42/4b in years 1996 and 1998, respectively (Wefer et al., 1997, 1998) (Table 1). The core sites were selected because they are located in the path of present-day dust plumes originating in the Sahara and hence the cores are expected to monitor changes in dust supply (Fig. 1). Furthermore, Core GeoB 5559-2 has been recovered from a seamount slope as far offshore as to avoid the effects of sediment transported by coastal currents, thus holding the best potential to record a pure eolian signal (Rea, 1994; Grousset et al., 1998).

Both cores were sampled on board with a resolution of 5 cm using syringes. Water content, porosity and density were measured on each sample by weighing a known volume of sediment (ranging between 8 and 10 ml) before and after drying at 80°C.

Grain-size distribution was measured after leaching the carbonate fraction with a pH ammonium acetate solution buffered at a pH of 4.0 and after oxidation of the organic matter with 10% H₂O₂. This carbonate-organic matter free fraction was analysed with a Coulter LS 100 laser particle size analyser (CLS), which is able to measure a wide range of particles (between 0.4 and 800 µm). CLS precision and accuracy were tested running several analyses with latex micro spheres of a known diameter and through replicate analyses that gave a coefficient of variation of 0.44%. The calculated parameters are the median and the ratio between the particles coarser than 2 µm and the total of particles.

Sediment samples for X-ray fluorescence analyses were ground and homogenised in an agate mortar. Glass discs were prepared for major element determination by fusing about 0.3 g of ground bulk sediment with a Li tetra borate flux. Pressing about 5 g of ground bulk sediment into a briquet, with boric acid backing, produced the discs for trace element analysis. Bulk sediment geochemistry of the samples was determined in a Philips PW 2400 sequential wavelength disperse X-ray spectrometer. The following major elements, Al, P, K, Ca, Si, Mn, Ti, Fe, Mg and Na, were calculated as oxides while the trace elements, Ba, Mo, Nb, Zr, Y, Sr, Th, Pb, Sn, Ce, Ga, Zn, W, Cu, Co, Ni, V were measured in ppm. After calibration with international standards (GSS-1 to GSS-7), the analytical precision was checked by replicate analyses of samples. This was found to be lower than 0.8% for major elements and about 4% for trace elements. All

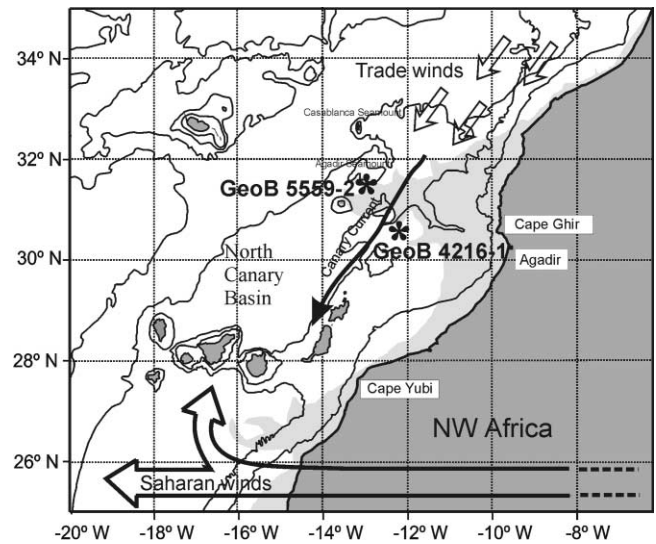


Fig. 1. Map of Northwest Africa showing the location of cores GeoB 5559-2 and GeoB 4216-1. Seasonal upwelling and filaments are outlined (light-shaded area) based on Van Camp et al. (1991), Hagen et al. (1996) and Davenport et al. (1999). Arrows indicate the average position of the present-day dominant wind systems and the Canary Current.

analyses were corrected for the contribution and dilution effect of the sea-salt content of the dried sediment. Results are presented after normalising the data to Al in order to account for the metal variations with respect to the variations of the aluminosilicate mineral fraction (Loring and Rantala, 1992).

4. Isotopic analyses and age model

Stable oxygen isotope measurements on fine fraction carbonate (< 38 µm) of Core GeoB 5559-2 were made on a Micromass PRISM (IRMS) mass spectrometer at the Geological Institute, ETH Zürich. Samples were homogenised by crushing before analysis. The analytical error of the internal lab standard was maximally $\pm 0.10\text{‰}$ for $\delta^{18}\text{O}$. All data are reported relative to the PDB standard.

Compositional variations within the fine fraction can significantly influence the stable isotopic stratigraphy measured on the nanofossil fraction. For example, Paull and Thierstein (1987) showed that oxygen and carbon isotopic ratios of individual splits of the < 38 µm fraction of deep-sea carbonate particles vary systematically with size over a range of 1.25–4.0‰. Low-diversity coccolith assemblage and other types of particles dominate

Table 1
Core data

Gravity core	Cruise	Longitude (N)	Latitude (W)	Depth (m)	Core length (cm)
GeoB 4216	M 37/1	30°37'8	12°23'7	3,178	1,117
GeoB 5559	M 42/4b	31°38'7	13°11'2	2,324	585

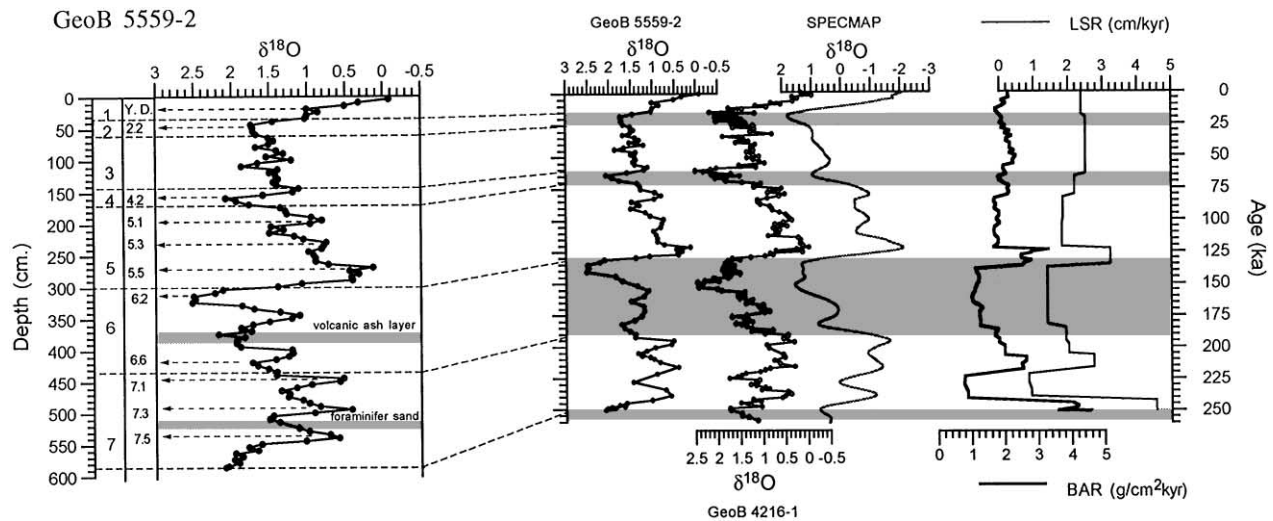


Fig. 2. Oxygen isotope records of GeoB 5559-2 plotted along core depth (cm) and age (kyr) axes. Age control points based on the stacked record of Martinson et al. (1987) are indicated (arrows). The small plateau in the $\delta^{18}\text{O}$ GeoB 5559-2 curve during the last deglaciation could correspond to the Younger Dryas (YD). The two intervals shaded (a volcanic ash layer and a foraminifera sand) were excluded before obtaining the age model to avoid interpretative errors. SPECMAP curve (Martinson et al., 1987) and *G. bulloides* $\delta^{18}\text{O}$ curve from GeoB 4216-1 (Freudenthal et al., 2001) are shown for comparison. Linear sedimentation rates (cm/kyr) and bulk accumulation rates ($\text{g}/\text{cm}^2\text{kyr}$) from GeoB 5559-2 are also represented.

Table 2

Age control points based on the stacked record of Martinson et al. (1987) for GeoB 5559-2. The corresponding isotopic events and linear accumulation rates are also represented. Stratigraphy from Core GeoB 4216-1 has been elaborated in Freudenthal et al. (2001)

GeoB 5559-2			
Depth (cm)	Age (kyr)	Event	LSR (cm/kyr)
48	17.85	2.2	2.39
158	64.09	4.2	2.50
193	79.25	5.1	2.19
228	99.38	5.3	1.84
268	123.82	5.5	1.82
313	135.10	6.2	3.21
418	183.3	6.6	1.38
443	196.06	7.1	1.92
493	215.54	7.3	2.73
538	240.19	7.5	0.91

most of these splits. However, empirical evidence from many cores suggests that the glacial–interglacial variability of the oxygen isotope signal dominates over possible compositional effects, and therefore raw fine fraction isotope data produce consistent isotope stratigraphy from which general paleoceanographic inferences can be made (Anderson and Steinmetz, 1981; Steinmetz and Anderson, 1984).

The age model of Core GeoB 5559-2 has been obtained from correlation between the measured $\delta^{18}\text{O}$ values and the well-dated SPECMAP $\delta^{18}\text{O}$ chronology (Fig. 2) (Imbrie et al., 1984; Pisias et al., 1984; Martinson et al., 1987). Ages of individual samples have been calculated by linear interpolation between the isotopic events shown in Table 2 and Fig. 2. Final correlation index between

SPECMAP and GeoB 5559-2 is 0.807. It results, then, that a sampling resolution of 5 cm corresponds in average to 2150 yr. The sedimentary record spans the last 250 kyr, from Oxygen Isotope Stages (OIS) 1–8. The age model of Core GeoB 4216-1, derived by correlating the $\delta^{18}\text{O}$ record measured on shells of planktic foraminifer-rich *Globigerina bulloides* with the SPECMAP record, was taken from Freudenthal et al. (2001).

5. Results

5.1. Sedimentological description and grain-size distribution

The lithology in cores GeoB 4216-1 and GeoB 5559-2 consists of nanofossil mud with foraminifer- and terrigenous-rich intervals (see core description chapters in Wefer et al., 1997, 1998). Visual examination evidenced a continuous sedimentation in Core GeoB 4216-1, except for an ash layer at 775 cm. The record in Core GeoB 5559-2 is interrupted in two intervals: a volcanic ash layer (between 380 and 390 cm) and a foraminifera sand (between 510 and 520 cm) (Fig. 2). In this area, this volcanic ash layer has also been found in several cores (Wefer et al., 1997). Since these intervals are sedimentological events with no climatic significance, samples from these layers were excluded from our results.

In order to study the wind strength variation, grain-size analyses were carried out in the lithogenic fraction (Sarnthein et al., 1981; Rea, 1994). After the statistical analysis (*k*-means clustering) samples can be grouped into two main families according to their grain-size

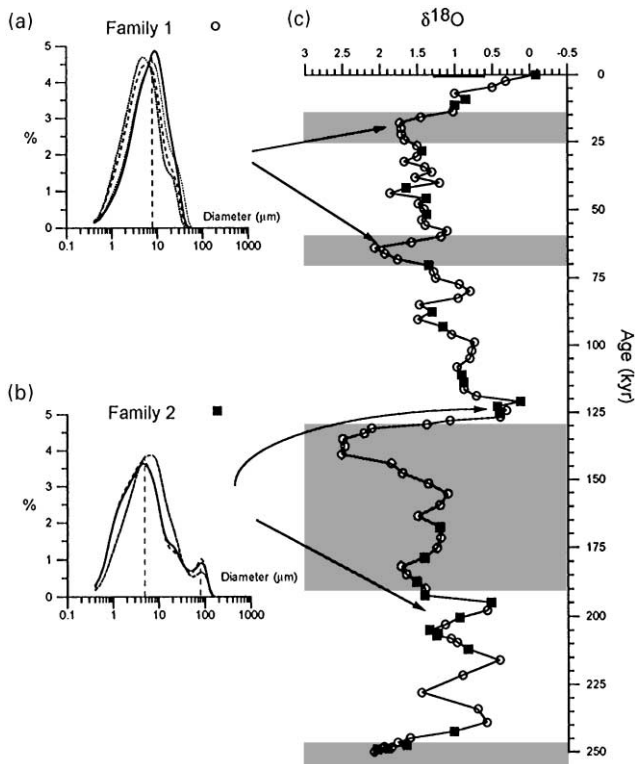


Fig. 3. Grain-size distribution of the carbonate-free fraction of samples from family 1 and 2 (a and b) from core GeoB 5559-2. Modes (also the secondary mode in the bi-modal distribution) are indicated with a vertical dashed line. (c) Temporal distribution of grain-size families. White dots: family 1 and black squares: family 2.

distribution although other statistically non-relevant sample typologies also exist (Fig. 3). Samples that belong to the 1st family are the most abundant (63.5%) and they are characterised by showing a unimodal distribution. In most of the samples, the mode is centred at 8 μm and a few samples present about 5% of particles over 63 μm diameter (Fig. 3a). The 2nd family constitutes 30% of the samples and displays a bi-modal distribution dominated by the finest fraction, with the mode centred at 5 μm . Sand content in this family is always less than 10% (Fig. 3b). The rest of the samples (6.5%) have a bi-modal distribution dominated by the coarsest fraction and belong to the 3rd family. As they correspond with the excluded intervals (the volcanic ash layer and the foraminifera sand) we have not used them in our study.

Grain-size families show a different distribution down-core (Fig. 3c). The most homogeneous intervals, formed only by the 1st family, correspond to full glacial conditions (OIS 2, 4 and 6), while interglacial periods (OIS 1 and 5) and also OIS 3 present samples from family 2 which occurs within intervals where samples from the 1st family dominate. Therefore, a clear glacial–interglacial control over the grain-size distribution can be observed in Core GeoB 5559-2.

Furthermore, grain-size distribution has been represented with a ratio that illustrates these glacial–interglacial variations. In this way, the coarse carbonate-free fraction, expressed here as (silt + sand)/total ratio, is significantly higher during full glacial conditions (OIS 2, 4 and 6) than during interglacials or OIS 3 (Fig. 4a). This parameter displays an increase during colder periods in within interglacial substages, as 5b, 5d, 7b and 7d. Events with coarser lithogenic particles coincide with glacial–interglacial transitions. Furthermore, the same pattern of variation is recorded by the median of this lithogenic fraction (Fig. 4b). Its values range between 6 and 12 μm during full glacial periods and terminations and between 4 and 6 μm in the rest of the record. Therefore, both parameters show the same glacial–interglacial variations with the coarser values at Terminations (I, II and maybe III) recorded in the core.

5.2. Geochemical markers

Geochemical parameters have been used successfully to evaluate the wind strength and the variations in dust input (Matthewson et al., 1995; Reichert et al., 1997). Here we use the Si/Al ratio as an indicator of terrigenous quartz input since in this region opal concentrations are very low (Neuer et al., 1997). Quartz from Northwest African sediments is mainly contained in the eolian lithogenic coarse fraction (Beltagy et al., 1972). Furthermore, Si concentration in the Saharan aerosol end-member is also higher in the coarser particles (Guiou and Thomas, 1996). Thus, Si/Al variations can be related to wind strength fluctuations (Boyle, 1983; Martinez et al., 1999).

Si/Al records in both cores have the same trend, however, Si/Al ratio in Core 4216-1 presents higher values (Fig. 4c). The results show that the pattern of the Si/Al curve in cores GeoB 5559-2 and GeoB 4216-1 (Fig. 4c) is very similar that the previously described for the grain-size parameters (Fig. 4a and b). Higher values are recorded during cold periods and lower values during warm stages (ranging from 2.5 in interglacial stages and OIS 3 to 3.2 at Terminations I, II and maybe III). This pattern is found also during colder periods in within interglacial stages (see OIS 5 and 7 in Fig. 4c) but the signal is weaker than during full glacial conditions. Maximum values of Si/Al ratio are reached at Terminations (I, II and maybe III) in the two studied cores. Since lithogenic coarse particles can be related to wind strength (Clemens, 1998), this implies that the wind strength in the NCB was increased at terminations.

As reported by Matthewson et al. (1995), aluminium concentration is taken as useful proxy of dust input in NW African margin because it is incorporated into fine-grained, wind-borne clays. In the studied cores, the Al concentrations presents a similar range of variation although somewhat higher values are shown in Core GeoB

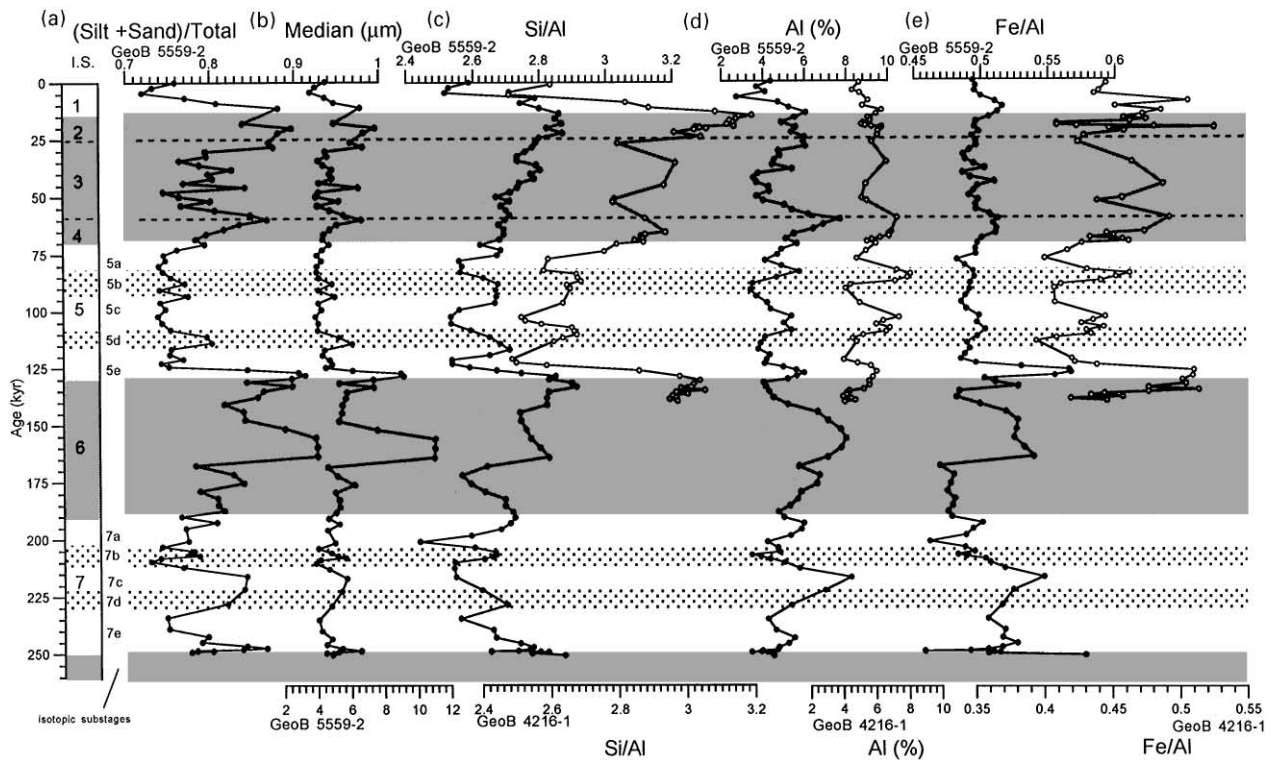


Fig. 4. Downcore profiles of (a) a grain-size parameter represented as (silt + sand)/total, (b) the median of the terrigenous fraction, (c) Si/Al ratio, as proxy indicators of wind stress, (d) the aluminium content (%) and (e) the Fe/Al ratio as proxy indicators of dust input to the North Canary Basin in GeoB 5559-2 (black dotted curves) and GeoB 4216-1 (white dotted curves). Geochemical study of Core GeoB 4216-1 has been carry out in the first 6 m. Glacial isotopic stages and substages are shaded.

4216-1 (Fig. 4d). Although aluminium concentrations are higher during full glacial periods, the general pattern does not show the same glacial–interglacial signal that Si/Al and grain-size proxies show. On the contrary, the smaller increments recorded appear with a cyclicity of 23 kyr (Fig. 4d). This result leads us to propose that the dust input in the NCB is related to the precessional insolation timing.

Since eolian dust from the Sahel region has a high content of iron oxides such as hematite and goethite (Balsam et al., 1995), the Fe/Al ratio may be used as a proxy for eolian particles (Bergametti et al., 1989). On the contrary, dust transported by the low-level trade winds is expected to have low Fe/Al values, since lateritic soils are lacking in the dust source. In Saharan aerosols collected in Barbados the Fe/Al ratio oscillates between summer and winter with a mean value of 0.58 (Arimoto et al., 1995). The Fe/Al ratio from an observed dustfall at 25°N of latitude is 0.54 (Game, 1962). The values in the records range from 0.45 in warm periods and up to 0.55 in the cold ones (Fig. 4e). The Fe/Al ratio and the aluminium both display a similar pattern coherent with a 23-kyr cyclicity. In both cores, GeoB 5559-2 and 4216-1, the Fe/Al ratio shows the same range of values (Fig. 4e). However, in Core 4216-1 the amplitude of variation is large. The aluminium concentration and the Si/Al ratio

(Fig. 4c and d) follow the same trend. Therefore, the Core GeoB 4216-1 record appears to be more sensitive to oscillations in dust input. This is probably due to its position along the path of the wind.

5.3. Spectral analyses

Spectral analyses of the records were carried with the Analyseries software package developed by Paillard et al. (1996) using the Blackman–Tuckey method. The results show the presence of the 100 kyr (eccentricity) and 23 kyr (precession) periods as the main cycles of temporal variability in the dust input to the North Canary Basin (Fig. 5). The two 100 kyr cycles present in the record can be identified by the strong peaks of (silt + sand)/total, the median and the Si/Al records at the end of glacial stages (Fig. 4a–c). On the other hand, Al concentration and Fe/Al ratio records vary with a 23-kyr cyclicity (Fig. 4d and e). The wind strength proxies (Si/Al ratio and grain-size parameters) also display a 23-kyr cycle but it is not the dominant frequency in those records.

Cross-spectral analysis on the dust proxies was carried out against the eccentricity–tilt–precession combination curve (ETP) (Imbrie et al., 1984). This curve is a normalised combination of the three orbital parameters and

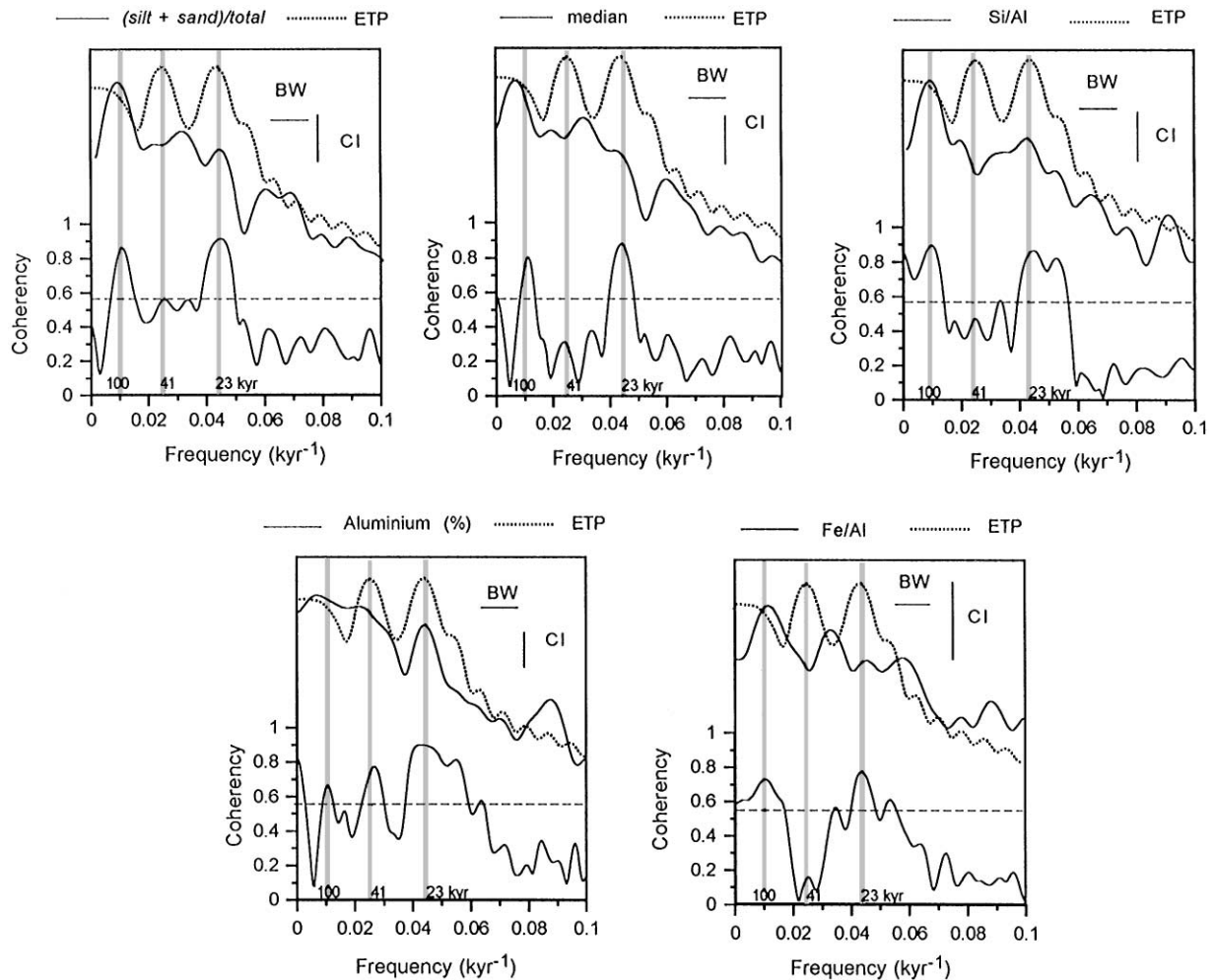


Fig. 5. Variance spectra of the core profiles shown in Fig. 4 (expressed as the logarithm of spectral power density versus frequency in cycles/kyr using the Blackman–Tuckey method) compared with the spectrum of ETP. The three main orbital periods of eccentricity (100 kyr), obliquity (41 kyr) and precession (23 kyr) are marked as vertical grey bands. The coherence plot indicates what frequency components are shared between the proxies and the ETP curve. An 80% confidence level is set, above which statistical significance in the coherence relationship is considered to exist (this level corresponds in this case with a coherency of 0.056). Bandwidth (BW) and 80% confidence interval (CI) are indicated with short horizontal and vertical segments, respectively.

can thus be used to compare variations in proxy records with orbitally induced changes in the amount of insolation (Matthewson et al., 1995). The cross-spectra of dust proxies (Al, Fe/Al, Si/Al and grain-size) also show maximum coherency at the 100 and 23 kyr periods (Fig. 5). Coherency and phase angle of these proxies with the ETP curve are represented in Table 3.

6. Discussion

Two issues should be considered to explain which was the forcing mechanism behind the supply of Saharan dust to the North Canary Basin: (i) the increase of Fe-and-Al-rich dust input at minima in the precessional index and (ii) the response of wind strength to the 100-kyr cycle. Both are discussed separately.

(i) Increase of Fe-and-Al-rich dust input at minima in the precessional index

Aluminium concentration and Fe/Al ratio are good indicators of dust input from the Northwest African margin, as they reflect Sahelian clays and laterites, respectively (Bergametti et al., 1989; Balsam et al., 1995; Matthewson et al., 1995). These proxies together with grain-size and Si/Al ratio, which are indicators of wind strength, vary with precession (Fig. 5). Maximum coherency with ETP for Al and Fe/Al is obtained at 23-kyr periods while for grain size and Si/Al this is at 100 kyr (Fig. 5). Therefore, the variation of dust supply into the NCB over the last 250 kyr is related to the precession insolation cycle while the wind strength is linked to the glacial–interglacial time scales.

Previous studies revealed a close relation between the increase in dust input in the tropical North Atlantic and

Table 3

Correlation and phase angle of the proxy records of dust in Core GeoB 5559-2 and TOC in Core GeoB 4216-1 with respect to ETP (Imbrie et al., 1984). Maximum Ice Volume ($\delta^{18}\text{O}$) is based on the SPECMAP curve. $\delta^{18}\text{O}$ values refer to measurements in Core GeoB 5559-2. Phase angle is shown for selected proxies (coherency with ETP higher than 0.6 at the 80% of confidence). (Si + Sa)/T is abbreviation for (silt + sand)/total

Period (kyr)	SPECMAP	$\delta^{18}\text{O}$	Al (%)	Fe/Al	Si/Al	Median	(Si + Sa)/T	TOC
<i>Correlation</i>								
100	0.92	0.85	0.65	0.72	0.89	0.75	0.84	0.89
41	0.86	0.78	0.67	0.13	0.46	0.31	0.54	0.75
23	0.92	0.94	0.89	0.77	0.85	0.87	0.90	0.91
<i>Phase angle</i>								
100	$-173 \pm 10^\circ$	$177 \pm 15^\circ$	$169 \pm 30^\circ$	$-108 \pm 24^\circ$	$-150 \pm 13^\circ$	$-163 \pm 22^\circ$	$-154 \pm 16^\circ$	$-145 \pm 12^\circ$
41	$-104 \pm 13^\circ$	$-87 \pm 18^\circ$	$-129 \pm 26^\circ$	—	—	—	—	$-80 \pm 23^\circ$
23	$-89 \pm 10^\circ$	$-119 \pm 9^\circ$	$14 \pm 13^\circ$	$13 \pm 21^\circ$	$-113 \pm 15^\circ$	$-87 \pm 14^\circ$	$-64 \pm 12^\circ$	$-40 \pm 11^\circ$

the increase in aridity in the Sahara (see for example Tiedemann et al., 1989). These studies linked a higher dust input into the basin with enhanced aridity during glacial periods (Sarnthein, 1978; Kolla et al., 1979). In addition, deMenocal et al. (1993b) suggest that glacial–interglacial variations in the North Atlantic SST field influence both dust source area aridity and the intensity of the dust-transporting trade winds. However, detailed studies showed that dust proxies vary with a 23 kyr periodicity (Pokras and Mix, 1985; Matthewson et al., 1995). These authors interpreted this periodicity to reflect aridity associated with the monsoon cycle. They further proposed that in periods with stronger monsoon, maxima of Northern Hemisphere seasonal insolation, extending to south Sahara and Sahel, the source area of dust was less dry and hence less of dust was available. In contrast, when monsoons were weaker at times of maxima in the precessional index, aridity increased together with dust availability.

In order to investigate the relation between dust-input proxies and precession we calculated phase angles (Fig. 6 and Table 3). Aluminium and Fe/Al ratio, which are indicating a Sahelian origin, appear in times of maxima Northern Hemisphere seasonal insolation, which means in phase with minima in the precessional index. As Fig. 7 shows, aluminium concentration and boreal summer insolation correlate peak to peak. However, these two signals are not highly coherent: the magnitude of the aluminium variation is greater during glacial periods concomitantly with lower amplitude of summer insolation fluctuation. This result may indicate that, although the 23-kyr cycle is driving dust supply to the NCB, a glacial–interglacial signal is also evident, as we discuss below.

As outlined in the introduction, two wind systems transport dust into the NCB, the trade winds and the SAL. The trade wind system is also driving and controlling the intensity of the summer upwelling in the NCB. Hence, if trade winds are related to dust supply and

upwelling, the precession signal should also be expected in the basin's productivity records. Freudenthal et al. (2001) in their study of Core GeoB 4216-1 showed that indeed the TOC record varies with precession (Fig. 7 and Table 3). The phase angles between TOC (taken as a productivity proxy) and ETP show that maximum productivity occurs in phase with minima in the precessional index (Fig. 6). This is the same relationship we found for the dust supply (Fig. 7).

A minimum in the precessional index implies high seasonality; this means warmer summers and colder winters (Kutzbach, 1981). Therefore, during warmer summers, with the ocean colder than land because of its higher thermal capacity, a strong thermal land–ocean contrast takes place. This leads to an intensification of the Azores high pressure over the ocean (H) (Fig. 8a). On the other hand, the higher insolation on the Sahara induces the development of a stronger low pressure over the continent (L). The strong pressure gradient between the high and the low is then expected to increase the strength of trade winds. Therefore, such scenario explains both the records of dust and productivity in terms of changes in trade wind intensity.

The problem with this interpretation is that it assumes all the dust derived from a northern source. However, the fact that dust from the equatorial latitude records also displays the same precession-related variations (Tiedemann et al., 1989; Matthewson et al., 1995; Flores et al., 2000), means that it is difficult to explain these records simply in terms of trade wind variations. Furthermore, cores at these latitudes also show precession-related variations in the fresh-water diatom record (Pokras and Mix, 1985, 1987). Clearly, the source of fresh-water diatoms is the dry lake beds from the Sahel region (Pokras, 1991; Gasse and Fontes, 1992). Therefore, their presence in the records cannot be related to the trade wind system.

During a minimum in the precessional index, the monsoonal system is enhanced owing to the maxima of

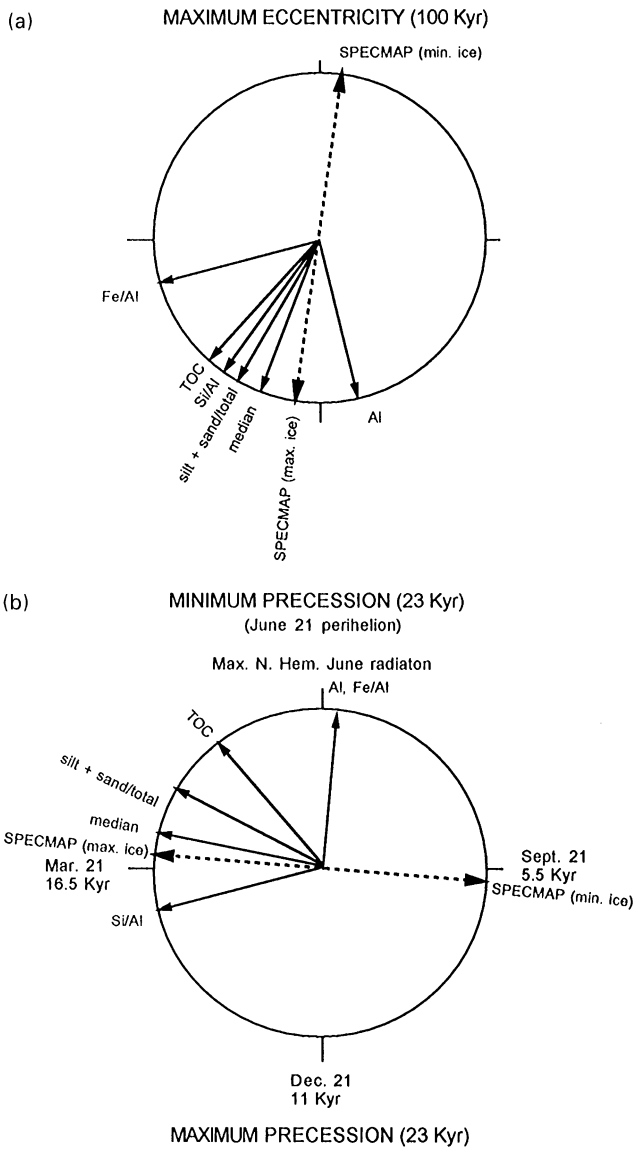


Fig. 6. Phase wheel summaries of insolation (represented as ETP variation), global ice volume (represented as the SPECMAP curve of Martinson et al., 1987) and proxy records of dust from GeoB 5559-2 and TOC from GeoB 4216-1. (A) Phase relationships at the eccentricity band. (B) Phase relationships at the precessional band. The obliquity parameter is not shown since none of the proxy records presents high coherence with that period. See Table 3 for the accurate phase angles.

Northern Hemisphere seasonal insolation (Kutzbach and Gallimore, 1988). The intensification of monsoonal winds weakens the Northern Hemisphere Trade winds at the equatorial latitudes (McIntyre et al., 1989). So that the Northern Trade winds cannot supply dust from the Sahel region to Equatorial latitudes. Such consideration opens another interpretation for the dust record of the NCB, which also can explain the records of Matthewson et al. (1995).

In a maxima of Northern Hemisphere seasonal insolation, the winter scenario is reverse with respect to the

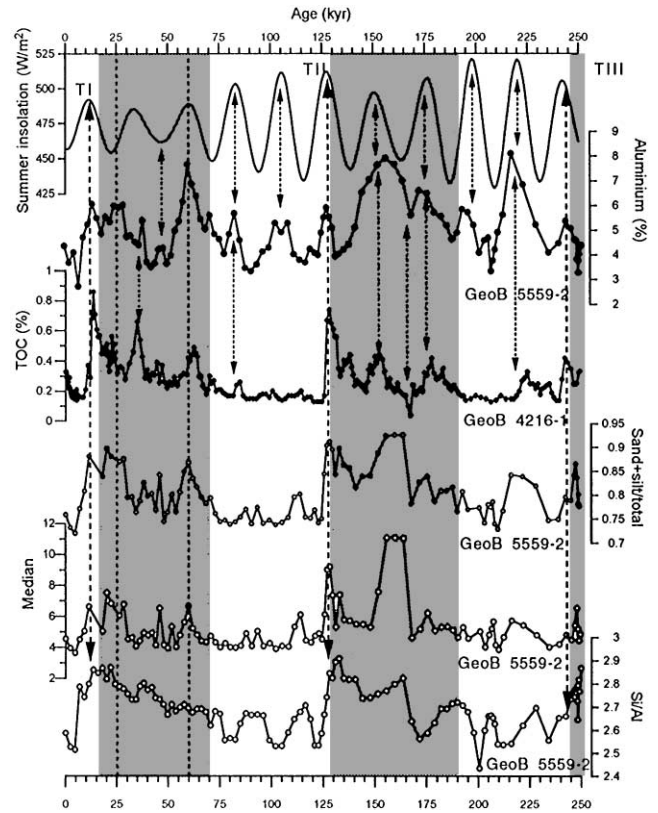


Fig. 7. Comparison among Al content, TOC percentages and proxies for wind strength (Si/Al and grain-size parameters) with the boreal summer insolation variation at 30°N (Berger, 1978). Glacial stages are shaded.

summer one. At this case, due to the ocean's higher thermal capacity than land, the summer Azores high, is shifted southwards and becomes very weak. Meanwhile, on the cooler continent a very strong high pressure develops (Fig. 8b). In this meteorological context, the SAL, and specially its northern branch, should be well developed, and thus may account for enhanced dust transport to the NCB.

Apparently, this model may be in contradiction with the fact that during a precession-minimum-summer, the monsoon regime is enhanced bringing rainfall to the Sahel region (Kutzbach, 1981; McIntyre et al., 1989). This increase is well documented in African lake level records (Kutzbach and Street-Perrott, 1985; Gasse et al., 1990; Street-Perrot and Perrot, 1990). Subsequently, the increased moisture would have reduced dust availability. Nevertheless, it is evident that an increase in moisture also implies a change in the weathering patterns. Rea (1994) concluded that in hyper-arid conditions (< 100 mm annual rainfall) dust generation falls off because the lack of moisture prevents the break down of the large minerals into clays of a size suitable for long-distance transport. In this case, an enhanced monsoon, which probably extended to the Sahel area, may have

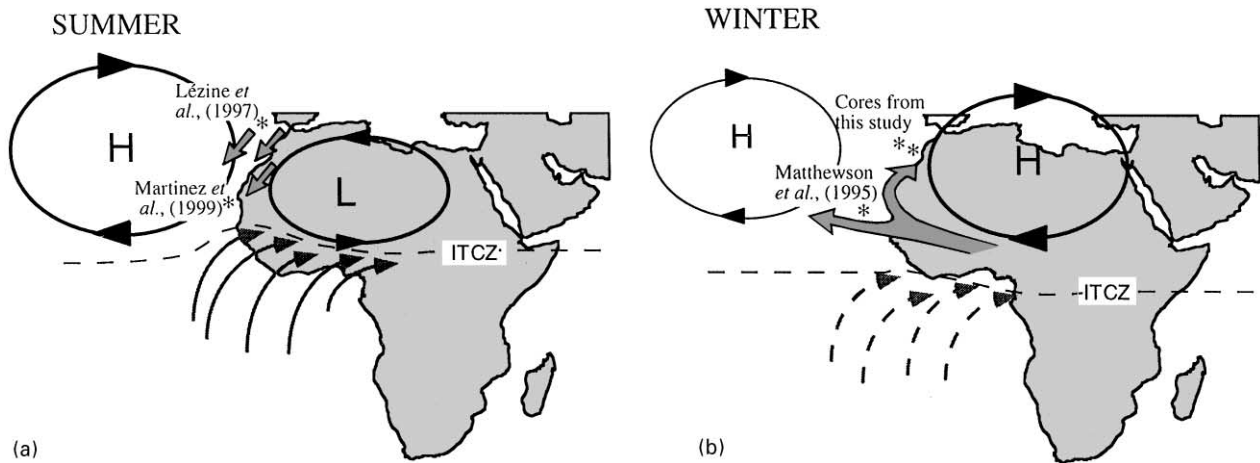


Fig. 8. Inferred climate scenarios at precession minimum (see text for explanation): (a) summer, (b) winter. Grey arrows represent dust-bearing wind systems: the trade winds and the SAL; black arrows represent the monsoon winds; weaker winds are shown by dashed arrows. Cores from this study and other cores cited in the text are indicated by asterisks.

provided enough moisture to increase significantly dust generation, and therefore dust availability. The dust would then be transported by the Saharan winds to the NCB. Furthermore, a grass Savannah vegetation type such as it is today in the Sahel area (White, 1983) allows for dust generation. Since pollen studies from the region show the presence of this vegetation type over the last 250 kyr (Hooghiemstra, 1996), it is suggested that monsoon rainfall, because of its seasonality, may be insufficient to develop a more permanent type of vegetation cover. This is inferred from the fact that grass Savannah spreads northwards into the Sahara reacting to moisture, while the Guinean rain forest belt did not shift beyond 15°N latitude (Hooghiemstra, 1996). According to the data set compiled by Hoelzmann et al. (1998) the boundary between steppe and savanna vegetation at 6000 yr BP (maxima seasonal insolation) occurred at 20°N which allows dust generation in the Sahel region. In the suggested model, the high seasonality typical during minima in the precessional index, may have contributed in establishing suitable conditions, first for weathering in summer and second for deflation by the Saharan winds in winter. Thus, the Sahel region can be considered a permanent source of dust.

Therefore, the record of dust supply into the NCB can be interpreted as the result of combining two meteorological scenarios, a winter and a summer one, both linked to minima in the precessional index. The summer scenario of enhanced trade winds explains the productivity variations and may also account for part of the dust signal while the winter scenario can explain most of the variation in dust supply. However, by means of frequency analysis we have found that some of the studies proxies (Si/Al ratio and grain-size parameters) have a clear response to the eccentricity cycle (100 kyr). In addition, productivity results in several cores from the NCB also display this glacial–interglacial signal (Freudenthal et al.,

2001; Moreno et al., 2000). Productivity signal in this area is linked to the trade wind system, by means of upwelling intensification. Therefore, we will discuss the importance of this cyclicity in our proxy records to understand the trade winds system variability over the last 250 kyr.

(ii) Response of wind strength to the 100-kyr cycle

Grain-size parameters, Si/Al ratio and grain-size families display a clear glacial–interglacial pattern of variation. On average, maximum values of these proxies appear associated with OIS 2, 4 and 6. In addition, Si/Al ratio and the grain-size parameters present mainly a 100-kyr response. However, these proxies are not in phase with the glacial maximum. On the contrary, they appear between 3000 and 6000 years after maximum ice conditions in the eccentricity wheel (Fig. 6). Therefore, we propose that the variation in these proxy records may be related to any change that took place at terminations.

In principle, these grain-size variations might be coupled with changes in the sedimentation patterns during glacial–interglacial transitions. Higher rates of sea-level rise occur at terminations (Shackleton, 1987). Besides the common turbidite deposition during sea-level lowstands, turbidite systems are observed to occur during sea-level rise (Prins and Postma, 2000). Therefore, we may consider that coarse particles deposited at the shelf edge may have advected via turbidites to the NCB at terminations. However, from the fact that both cores record the same events and Core GeoB 5559-2 is located in the slope of a seamount, any influence from the shelf in the core records seems unlikely.

Arguably, the observed grain-size variations can be interpreted as related to changes in the energy of the transporting wind (Rea, 1994). Sarnthein et al. (1981) and Grousset et al. (1998) found glacial–interglacial patterns of variation in their records, south of the Canary Islands.

They concluded that the increase in the particles grain size during full glacial conditions was related to higher trade wind intensities. However, the coarsest grain sizes and the higher values in the Si/Al ratio are recorded at terminations and not at glacial maxima in the studied cores from the NCB (Fig. 4). Although the overall pattern is an increase in the dust proxies during glacial stages, superimposed to this signal there is a significant increment of the wind strength proxies at Terminations.

As discussed before, wind and productivity are linked to trade wind strength. In Fig. 7 the TOC record from Core GeoB 4216-1 is represented and compared with dust proxies and summer insolation at 30°N. The %TOC record contains an intermediate mixture of the 23-kyr proxies (%Al, Fe/Al ratio) and the 100-kyr proxies (grain-size parameters and Si/Al ratio). This may indicate that, although the precessional pattern is evident, the glacial–interglacial signal is influencing trade winds variations. Consequently, a good correlation between grain-size and Si/Al ratio and peaks in the TOC record is shown (Fig. 7). Therefore, the trade winds in this region were strongly intensified at the terminations. This conclusion is strengthened by the results from different authors around this area. Thus, Lézine and Denèfle (1997) produced a detailed pollen records for Termination I from a core from offshore Portugal and concluded that anticyclonic circulation was strengthened over the Northeastern Atlantic. They further stated that cooler sea surface temperatures (SST) were coeval with stronger trade winds. After a palynological study from a core located offshore Morocco, Marret and Turon (1994) postulated an enhancement in trade winds strength during last deglaciation. South of the Canary Islands Martinez et al. (1999) and Ternois et al. (2000) also found an increase in grain-size and productivity proxies at Termination I, which they related to trade wind intensity (Fig. 8a).

Terminations are unique intervals of climate change, in which climate switches from a glacial to an interglacial mode. In these intervals, maxima in boreal summer insolation, rapid ice-sheet melting and fast rates of sea-level rise concur. Hughen et al. (1996) and Overpeck et al. (1989) proposed that under this scenario the North Atlantic SST lowered by the melt water, may have strengthened the high-pressure system over the North Atlantic. Therefore, SST variations in the North Atlantic provide a mechanism to explain changes in trade wind intensity. Moreover, this conclusion reinforces previous ideas on how SST changes in North Atlantic have influence upon the African climate (deMenocal, 1995).

7. Conclusion

This paper shows that precession and eccentricity cycles play a role in driving changes in dust input to the North Canary Basin. The record of dust can be inter-

preted in terms of a summer and a winter scenario during a minimum in the precessional index. During summers, trade winds were intensified which resulted in higher productivity and the transport of coarser grains from a Northwest African source. Meanwhile, in the Sahel area conditions were suitable for increased dust generation. During winter, the Saharan Air Layer could transport this dust to the NCB.

Superimposed to the overall pattern of a trade winds enhancement during glacial periods, maxima in productivity and grain-size both appear at Terminations I–III. At these periods of higher insolation but lower SST over the North Atlantic, the subtropical anticyclonic circulation may have intensified. Then, the strengthened trade winds forced upwelling and had the ability to carry coarser particles at terminations.

Acknowledgements

We gratefully acknowledge the officers and crew of the R/V Meteor for technical support during the CANIGO cruises (December 1996 and October 1998) and people from Bremen University, Geological Institute of Lisbon and Geological Institute of Zurich for their help in sampling and description of sediment cores. We thank E. Segui, J.M. Socias (XRF laboratory) and P. Hortolà, M. Guart (Sedimentological laboratory) for laboratory analyses. We sincerely thank I. Cacho and J. Villanueva (Institute of Chemical and Environmental Research, CSIC, Barcelona), L. Dupont (University of Bremen), P. Bertrand, P. Martinez and F. Grousset (University of Bordeaux) for useful comments on an earlier version of the manuscript. Prof. J. Rose and B. Ruddiman reviewed the manuscript and provided helpful suggestions. The present study was supported by the CANIGO project (MAS3-CT9-0060) and a Comissionat d'Universitats i Recerca fellowship (Ana Moreno).

References

- Anderson, T.F., Steinmetz, J.C., 1981. Isotopic and biostratigraphical records of calcareous nannofossils in a Pleistocene core. *Nature* 294, 741–744.
- Arimoto, R., Duce, R.A., Ray, B.J., Ellis, W., Cullen, J.D., Merrill, J.T., 1995. Trace elements in the atmosphere over the North Atlantic. *Journal of Geophysical Research* 100, 1199–1213.
- Balsam, W.L., Otto-Bliesner, B.L., Deaton, B.C., 1995. Modern and last glacial maximum eolian sedimentation patterns in the Atlantic Ocean interpreted from sediment iron oxide content. *Paleoceanography* 10, 493–507.
- Beltagy, A.I., Chester, R., Padgham, R.C., 1972. The particle-size distribution of quartz in some North Atlantic deep-sea sediments. *Marine Geology* 13, 297–310.
- Bergametti, G., Gomes, L., Coudé-Gaussen, G., Rognon, P., Le Coustumer, M.N., 1989. African dust observed over Canary Islands: source-regions identification and transport pattern for some summer situations. *Journal of Geophysical Research* 94, 14,855–14,864.

- Berger, A., 1978. Long-term variations of caloric insolation resulting from the Earth's orbital elements. *Quaternary Research* 9, 139–167.
- Bertrand, P., Shimmield, G.B., Martinez, P., Grousset, F.E., Jorissen, F., Paterne, M., Pujol, C., Bouloubassi, I., Buat-Menard, P., Peyrouquet, J.-P., Beaufort, L., Sicre, M.-A., Lallier-Verges, E., Foster, J.M., Ternois, Y., 1996. The glacial ocean productivity hypothesis: the importance of regional temporal and spatial studies. *Marine Geology* 130, 1–9.
- Boyle, E., 1983. Chemical accumulation variations under the Peru current during the past 130,000 years. *Journal of Geophysical Research* 88, 7667–7680.
- Bustos, J.J., Cuevas, E., Marrero, C., Afonso, S., 1998. Fenómenos y sistemas meteorológicos: caracterización de masas de aire en la troposfera libre y en la capa de mezcla en Canarias. IX Asamblea Nacional de Geodesia y Geofísica, Aguadulce, Almería.
- Chiapello, I., Bergametti, G., Chatenet, B., 1997. Origins of African dust transported over the northeastern tropical Atlantic. *Journal of Geophysical Research* 102, 13,701–13,709.
- Clemens, C., 1998. Dust response to seasonal atmospheric forcing: proxy evaluation and calibration. *Paleoceanography* 13, 471–490.
- Clemens, C., Prell, W., 1990. Late Pleistocene variability of Arabian Sea summer monsoon winds and continental aridity: eolian records from the lithogenic component of deep-sea sediments. *Paleoceanography* 5, 109–145.
- Davenport, R., Neuer, S., Hernández-Guerra, A., Ruedas, M.J., Llinas, O., Fischer, G., Wefer, G., 1999. Seasonal and interannual pigment concentration in the Canary Islands region from CZCS data and comparison with observations from the ESTOC. *International Journal of Remote Sensing* 20, 1419–1433.
- deMenocal, P., 1995. Plio-Pleistocene African climate. *Science* 270, 53–59.
- deMenocal, P., Rind, D., 1993a. Sensitivity of Asian and African climate to variations in seasonal insolation, glacial ice cover, sea surface temperature and Asian orography. *Journal of Geophysical Research* 98, 7265–7287.
- deMenocal, P., Ruddiman, W., Pokras, E.M., 1993b. Influences of high- and low-latitude processes on African terrestrial climate: Pleistocene eolian records from equatorial Atlantic Ocean Drilling Program site 663. *Paleoceanography* 8, 209–242.
- Flores, J.A., Bárcena, M.A., Sierro, F.J., 2000. Ocean-surface and wind dynamics in the Atlantic Ocean off Northwest Africa during the last 140,000 years. *Palaeogeography, Palaeoclimatology, Palaeoecology*, 161, 3–4, 459–478.
- Freudenthal, T., Meggers, H., Henderiks, J., Kuhlmann, H., Moreno, A., Wefer, G., 2001. Variability of upwelling intensity and filament activity off Morocco during the last 250,000 years. *Deep Sea Research, II*, in press.
- Fütterer, D.K., 1983. The modern upwelling record off NW Africa. In: Thiede, J., Suess, E. (Eds.), *Coastal Upwelling: its Sediment Record*. NATO Advanced Research Institute. Plenum Press, New York, pp. 105–121.
- Gabric, A.J., García, L., Van Camp, L., Nykjaer, L., Eifler, W., Schrimpf, W., 1993. Offshore export of shelf production in the Cape Blanc (Mauritania) giant filament as derived from coastal zone color scanner imagery. *Journal of Geophysical Research* 98, 4697–4712.
- Game, P.M., 1962. Observations on a dustfall in the Eastern Atlantic. *Journal of Sedimentary Petrology* 34, 355–359.
- Gasse, F., Fontes, J.C., 1992. Climatic changes in northwest Africa during the last deglaciation, 16–7 ka BP. In: Bard, E., Broecker, W.S. (Eds.), *The Last Deglaciation: Absolute and Radiocarbon Chronologies*, Vol. 12. Springer, Berlin, pp. 295–325.
- Gasse, F., Stabell, B., Fourtanier, E., Van Iperen, Y., 1989. Freshwater diatom influx in Intertropical Atlantic: relationships with continental records from Africa. *Quaternary Research* 32, 229–243.
- Gasse, F., Tehet, R., Durand, A., Gibert, E., Fontes, J.-C., 1990. The arid-humid transition in the Sahara and the Sahel during the last deglaciation. *Nature* 346, 141–146.
- Gelado-Caballero, M.D., Pérez, E., Collado, C., Hernández-Brito, J.J., 2001. Variability of dust inputs to the CANIGO zone. *Deep Sea Research, II*, in press.
- Grousset, F.E., Parra, M., Bory, A., Martinez, P., Bertrand, P., Shimmield, G.B., Ellam, R.M., 1998. Saharan wind regimes traced by the Sr-Nd isotopic composition of subtropical Atlantic sediments: last Glacial maximum vs today. *Quaternary Science Reviews* 17, 395–409.
- Guieu, C., Thomas, J., 1996. Saharan aerosols: from the soil to the ocean. In: Guerzoni, S., Chester, R. (Eds.), *The Impact of Desert Dust across the Mediterranean*. Kluwer Academic Publishers, Dordrecht, pp. 207–216.
- Hagen, E., Züllicke, C., Feistel, R., 1996. Near-surface structures in the Cape Ghir filament off Morocco. *Oceanologica Acta* 19, 577–597.
- Hoelzmann, P., Jolly, D., Harrison, S.P., Laarif, F., Bonnefille, R., Pachur, H.-J., 1998. Mid-Holocene land-surface conditions in northern Africa and the Arabian peninsula: a data set for the analysis of biogeophysical feedbacks in the climate system. *Global Biogeochemical Cycles* 12, 35–51.
- Hooghiemstra, H., 1989. Variations of the NW African trade wind regime during the last 140,000 years: changes in pollen flux evidenced by marine sediment records. In: Leinen, M., Sarnthein, M. (Eds.), *Paleoclimatology and Paleometeorology: Modern and Past Patterns of Global Atmospheric Transport*, NATO ASI Series. Kluwer, Dordrecht, pp. 733–770.
- Hooghiemstra, H., 1996. Aspects of Neogene-Quaternary environmental and climatic change in equatorial and Saharan Africa. *Palaeoecology of Africa* 24, 115–132.
- Hooghiemstra, H., Stalling, H., Agwu, C.O.C., Dupont, L.M., 1992. Vegetational and climatic changes at the northern fringe of the Sahara 250,000–5,000 years BP: evidence from 4 marine pollen records located between Portugal and the Canary Islands. *Review of Palaeobotany and Palynology* 74, 1–53.
- Hughen, K.A., Overpeck, J.T., Peterson, L.C., Trumbore, S., 1996. Rapid climate changes in the tropical Atlantic region during the last deglaciation. *Nature* 380, 51–54.
- Imbrie, J., Hays, J.D., Martinson, D.G., McIntyre, A., Mix, A.C., Morley, J.J., Pisias, N.G., Prell, W.L., Shackleton, N.J., 1984. The orbital theory of Pleistocene climate: support from a revised chronology of the marine $\delta^{18}\text{O}$ record. In: Berger, A. (Ed.), *Milankovitch and Climate, Proceedings of the NATO Advanced Research Workshop on Milankovitch and Climate*. D. Reidel Publishing Company, Palisades, New York, pp. 269–305.
- Klein, B., Siedler, G., 1989. On the origin of the Azores current. *Journal of Geophysical Research* 94, 6159–6168.
- Kolla, V., Biscaye, P., Hanley, A.F., 1979. Distribution of quartz in late Quaternary Atlantic sediments in relation to climate. *Quaternary Research* 11, 261–277.
- Kutzbach, J.E., 1981. Monsoon climate of the Early Holocene: climate experiment with the Earth's orbital parameters for 9000 years ago. *Science* 214, 59–61.
- Kutzbach, J.E., Gallimore, R.G., 1988. Sensitivity of a coupled atmosphere/mixed layer ocean model to changes in orbital forcing at 9,000 years B.P. *Journal of Geophysical Research* 93, 803–821.
- Kutzbach, J.E., Street-Perrott, F.A., 1985. Milankovitch forcing of fluctuations in the level of tropical lakes from 18 to 0 kyr BP. *Nature* 317, 130–134.
- Lamb, H., Gasse, F., Benkaddour, A., El Hamouti, N., Van der Kaars, S., Perkins, W.T., Pearce, N.J., Roberts, C.N., 1995. Relation between century-scale Holocene arid intervals in tropical and temperate zones. *Nature* 373, 134–137.
- Loring, D.H., Rantala, R.T.T., 1992. Manual for the geochemical analyses of marine sediments and suspended particulate matter. *Earth Science Reviews* 32, 235–283.

- Lézine, A.M., Denèfle, M., 1997. Enhanced anticyclonic circulation in the eastern North Atlantic during cold intervals of the last deglaciation inferred from deep-sea pollen records. *Geology* 25, 119–122.
- Marret, F., Turon, J.L., 1994. Paleohydrology and paleoclimatology off Northwest Africa during the last glacial–interglacial transition and the Holocene: Palynological evidences. *Marine Geology* 118, 107–117.
- Martinez, P., Bertrand, P., Shimmield, G.B., Cochrane, K., Jorissen, J., Foster, J.M., Dignan, M., 1999. Upwelling intensity and ocean productivity changes off Cape Blanc (Northwest Africa) during the last 70,000 years: geochemical and micropalaeontological evidence. *Marine Geology* 158, 57–74.
- Martinson, D.G., Pisias, N.G., Hays, J.D., Imbrie, J., Moore, T.C., Shackleton, N.J., 1987. Age dating and the orbital theory of the Ice Ages: development of a high-resolution 0 to 300,000-year chronostratigraphy. *Quaternary Research* 27, 1–29.
- Matthewson, A.P., Shimmield, G.B., Kroon, D., Fallick, A.E., 1995. A 300 kyr high-resolution aridity record of the North African continent. *Paleoceanography* 10, 677–692.
- McIntyre, A., Ruddiman, W., Karlin, K., Mix, A.C., 1989. Surface water response of the equatorial Atlantic ocean to orbital forcing. *Paleoceanography* 4, 19–55.
- Mittelstaedt, E., 1983. The upwelling area off northwest Africa — a description of phenomena related to coastal upwelling. *Progress in Oceanography* 12, 307–331.
- Moreno, A., Targarona, J., Nave, S., Kuhlmann, H., Freudenthal, T., Canals, M., Abrantes, F., 2001. Productivity response in the North Canary Basin to Trade wind intensity variations during the last 250,000 years, in preparation.
- Neuer, S., Ratmeyer, V., Davenport, R., Fischer, G., Wefer, G., 1997. Deep water particle flux in the Canary Island region: a seasonal trends in relation to long-term satellite derived pigment data and lateral sources. *Deep-Sea Research I* 44, 1451–1466.
- Overpeck, J.T., Peterson, L.C., Kipp, N., Imbrie, J., Rind, D., 1989. Climate change in the circum-north Atlantic region during the last deglaciation. *Nature* 338, 553–557.
- Paillard, D., Labeyrie, L., Yiou, P., 1996. Macintosh program performs time-series analysis. *Eos Transactions* 77, 379.
- Parkin, D.W., Shackleton, N.J., 1973. Trade wind and temperature correlations down a deep-sea core off the Saharan coast. *Nature* 245, 455–457.
- Paull, C.K., Thierstein, H.R., 1987. Stable isotopic fractionation among particles in Quaternary coccolith-size deep-sea sediments. *Paleoceanography* 2, 423–429.
- Pisias, N.G., Martinson, D.G., Moore, T.C., Shackleton, N.J., Prell, W., Hays, J.D., Boden, G., 1984. High resolution stratigraphic correlation of benthic oxygen isotopic records spanning the last 300,000 years. *Marine Geology* 56, 119–136.
- Pokras, E.M., 1991. Source areas and transport mechanisms for freshwater and brackish-water diatoms deposited in pelagic sediments of the Equatorial Atlantic. *Quaternary Research* 35, 144–156.
- Pokras, E.M., Mix, A., 1985. Eolian evidence for spatial variability of Late Quaternary climates in Tropical Africa. *Quaternary Research* 24, 137–149.
- Pokras, E.M., Mix, A.C., 1987. Earth's precession cycle and Quaternary climatic change in tropical Africa. *Nature* 326, 486–487.
- Prins, M., Postma, G., 2000. Effects of climate, sea level, and tectonics unraveled for last deglaciation turbidite records of the Arabian Sea. *Geology* 28, 375–378.
- Prospero, J.M., 1996. Saharan dust transport over the North Atlantic ocean and Mediterranean: an overview. In: Guerzoni, S., Chester, R. (Eds.), *The Impact of Desert Dust Across the Mediterranean*. Kluwer Academic Publisher, Dordrecht, pp. 133–151.
- Rea, D., 1994. The paleoclimatic record provided by eolian deposition in the deep sea: the geologic history of wind. *Reviews of Geophysics* 32, 159–195.
- Reichert, G., den Dulk, M., Visser, H.J., van der Weijden, C.H., Zachariasse, W.J., 1997. A 225 kyr record of dust supply, paleoproductivity and the oxygen minimum zone from the Murray Ridge (northern Arabian Sea). *Paleogeography, Palaeoclimatology, Palaeoecology* 134, 149–169.
- Ruddiman, W., 1997. Tropical Atlantic terrigenous fluxes since 25,000 yrs B. P. *Marine Geology* 136, 189–207.
- Sarnthein, M., 1978. Sand deserts during glacial maximum and climatic optimum. *Nature* 272, 43–46.
- Sarnthein, M., Koopmann, B., 1980. Late Quaternary deep-sea record on northwest African dust supply and wind circulation. *Paleoecology of Africa* 12, 239–253.
- Sarnthein, M., Tetzlaff, G., Koopmann, B., Wolter, K., Pflaumann, U., 1981. Glacial and interglacial wind regimes over the eastern subtropical Atlantic and North-West Africa. *Nature* 293, 193–196.
- Sarnthein, M., Thiede, J., Pflaumann, U., Erlenkeuser, H., Fütterer, D., Koopmann, B., Lange, H., Seibold, E., 1982. Atmospheric and oceanic circulation patterns off Northwest Africa during the past 25 million years. In: Rad, U., Hinz, I., Sarnthein, M., Seibold, E. (Eds.), *Geology of the Northwest Africa Continental Margin*. Springer-Verlag, New York, pp. 547–604.
- Schütz, L., Jaenicke, R., Pietrek, H., 1981. Saharan dust transport over the North Atlantic Ocean. In: Pèwè, T. (Ed.), *Desert Dust: Origin, Characteristics and Effect of Man*, Vol. 186, Special Paper. Geological Society of America, Boulder, pp. 87–100.
- Shackleton, N.J., 1987. Oxygen isotopes, ice volume and sea level. *Quaternary Science Reviews* 6, 183–190.
- Stein, R., 1985. Late Neogene changes of Paleoclimate and Paleoproductivity off Northwest Africa. *Paleogeography, Palaeoclimatology, Palaeoecology* 49, 47–59.
- Steinmetz, J.C., Anderson, T.F., 1984. The significance of isotopic and paleontologic results on Quaternary calcareous nannofossil assemblages from Caribbean core P6304-4. *Marine Micropaleontology* 8, 403–424.
- Street-Perrot, F.A., Perrot, R.A., 1990. Abrupt climate fluctuations in the tropics: the influence of Atlantic Ocean circulation. *Nature* 343, 607–612.
- Ternois, Y., Sicre, M.-A., Paterne, M., 2000. Climatic changes along the northwest African continental margin over the last 30 kyr. *Geophysical Research Letters* 27, 133–136.
- Tetzlaff, G., Wolter, K., 1980. Meteorological patterns and the transport of mineral dust from the north African continent. *Paleoecology of Africa* 12, 31–42.
- Tiedemann, R., Sarnthein, M., Stein, R., 1989. Climatic changes in the Western Sahara: aeolo-marine sediment record of the last 8 million years (sites 657–661). In: Ruddiman, W., Sarnthein, M. (Eds.), *Proceedings of the Ocean Drilling Program, Scientific Results*, Vol. 108, pp. 241–261.
- Van Camp, L., Nykjaer, L., Mittelstaedt, E., Schlittenhardt, P., 1991. Upwelling and boundary circulation off Northwest Africa as depicted by infrared and visible satellite observations. *Progress in Oceanography* 26, 357–402.
- Wefer, G., Abrantes, F., cruise participants, 1997. Report and Preliminary Results of METEOR-Cruise M 37/1, Lisbon-Las Palmas, 04 December–23 December 1996. *Berichte, Fachbereich Geowissenschaften, Universität Bremen, Bremen*, 79pp.
- Wefer, G., Segl, M., cruise participants, 1998. Report and Preliminary Results of METEOR-Cruise M 42/4, Las Palmas-Viena do Castelo, 26 September–26 November 1998. *Berichte, Fachbereich Geowissenschaften, Universität Bremen, Bremen*, 104pp.
- White, F., 1983. *The Vegetation of Africa*. UNESCO, Paris, 356pp.
- Wooster, W.S., Bakun, A., McLain, D.R., 1976. The seasonal upwelling cycle along the eastern boundary of the North Atlantic. *Journal of Marine Research* 34, 131–141.